View metadata, citation and similar papers at core.ac.uk
brought to you by CORE
provided by CiteSeerX

IMAGING OF PORE SCALE DISTRIBUTION OF FLUIDS AND WETTABILITY

Munish Kumar, Tim Senden, Mark A. Knackstedt, Shane J. Latham, Val Pinczewski, Robert M. Sok, Adrian P. Sheppard & Michael L. Turner
Department of Applied Mathematics, Australian National University, Canberra, Australia
School of Petroleum Engineering, University of NSW, Sydney, Australia

This paper was prepared for presentation at the International Symposium of the Society of Core Analysts held in Abu Dhabi, UAE 29 October-2 November, 2008

ABSTRACT

Wettability has a profound effect on reservoir recovery and productivity. It determines the microscopic distribution of fluids in the pore-space which, in turn, determine important global multiphase properties such as capillary pressure, relative permeability, residual saturation and resistivity index. Complexities in pore-space geometry, rock-fluid and fluid-fluid interactions have limited descriptions of wettability to highly simplified model systems and wettability in real porous systems remains a poorly understood phenomenon.

This paper utilizes two new techniques which have the potential to greatly improve our understanding of wettability in real porous systems. The first is a technique to reproducibly clean and modify the surface energy of clastic and carbonate cores to produce well defined wettability states. The second is a technique for directly imaging the pore-scale distribution of fluids in reservoir cores using high resolution tomography and a newly developed 3D registration technique which allows voxel perfect alignment of a set of images of the same core. We present results for a preliminary study of drainage and imbibition in Fontainebleau sandstone, sucrosic dolomite and oomoldic grainstone cores at well defined wettability states using air and water to demonstrate the applicability of the techniques.

The imaged fluid distributions show that gas is preferentially located in larger pores with water occupying smaller pores. The gas saturations measured compare well with those calculated from the imaged fluid distributions. The imaged pore-scale fluid distributions are also compared with predictions based on computations made directly on dry images of the pore-space and in equivalent network models. The computations use simple percolation concepts to model the pore-scale distributions. Drainage saturations and fluid distributions compare well with invasion percolation. Imbibition fluid distributions compare well with ordinary percolation. The comparisons show, for the first time, the feasibility of testing the validity of network models for multi-phase flow by directly comparing model fluid saturations with imaged saturations in real systems on a pore-to-pore basis.

INTRODUCTION

Wettability in real porous systems remains a poorly understood phenomenon as it is very difficult to measure and characterize. Commonly used single global measures such as the Amott-Harvey and USBM (Anderson, 1987) indices (WI) are clearly limited in their ability to describe the rich variety of multi-phase behaviour observed in real reservoir systems

(Morrow & Mason, 2001). A deeper understanding of wettability and its effect on multi-phase rock properties requires detailed knowledge of the pore-scale distribution of fluids at well defined wettability states. Previous attempts to produce well defined wettability states have been limited to simple model systems. Morgan & Pirson, 1964 varied the proportion of oil-wet and water-wet beads in a pack by treating a portion of the beads with a silane solution to render them oil wet. The remaining beads were untreated and water wet. By varying the proportion of beads, idealized core material of different wettability states was generated. In the following section we discuss a technique which allows the establishment of well defined water wet, mixed wet (fractional) and oil wet states in reservoir core material. The technique allows reproducible cleaning and modification of the surface energy of clastic and carbonate cores to establish different wetting states in the same core.

Following this we apply a newly developed image registration technique (Latham et al, 2008) which allows voxel perfect overlay of 3D tomographic images of the same core samples at different saturation states. This allows direct imaging of the fluid distribution in the pore-spaces of the same core in 3D under a range of wettability and saturation states; air/water drainage and imbibition studies are presented. Pore network partitioning methods are used to define local pore scale fluid distributions and individual pore occupancies. The imaged pore-scale fluid distributions are compared with predictions based on computations made directly on dry images of the pore-space and in equivalent network models. The comparisons show, for the first time, the feasibility of testing the validity of network models for multi-phase flow by directly comparing model fluid saturations with imaged saturations in real systems on a pore-to-pore basis.

CLEANING AND WETTABILITY ALTERATION OF CORES

Cleaning procedures begin with a regime of solvent washing to remove the bulk of the organics. However, flushing the core repeatedly with organic solvents does not guarantee that all contaminants will be removed and in all cases a thin film or monolayer will be left behind. Moreover, it is now recognised that solvent extraction redistributes contaminant onto uncontaminated surfaces. For example, Hirasaki et al, 1990 showed that traditional cleaning methods like Dean-Stark extraction do not produce water-wet conditions in cores that were initially not water-wet. Another critical step in any solvent cleaning procedure is the drying of the core and again this acts to redistribute contaminants (Zhang et al., 2006). Chemical treatments that oxidize or cleave monolayers on the rock surfaces damage or alter the core material; examples of damage include the etching, roughening or removal of core minerals.

In the present work we have used a vacuum process consisting of a cold electric plasma of water vapour that physically removes monolayers and renders the rock surface hydrophilic. Our plasma apparatus consists of a cylindrical glass vacuum chamber with an external antenna wrapped in a single loop around the mid-section. The stainless steel ends are earthed. A balanced load is transmitted through a pressure of between 0.1 to 0.2 torr water vapour for 3-15 min. The system is continuously pumped during the exposure. Within the water plasma highly reactive radical species and ions such as $H^{\bullet}$, H^{+}, OH^{-}, $OH^{\bullet}$, $O^{\bullet}$ and O^{+} react with the surface. Independent tests have shown that these short lived plasma

species penetrate at least 10 mm into the pore space of a rock. Most materials become highly hydroxylated which greatly increases their affinity to water. The energy of the plasma treatment means that no sputtering is likely and mass spectral analysis shows that only very light molecular fragments such as CO are liberated from an organically contaminated surface. In this way molecularly thin films are oxidized and evaporate as gaseous molecules. Further details are given in (Kumar et al., 2008).

The method does not remove macroscopic thick films greater than several hundred nanometres, however, these films are rendered hydrophilic. The permanency of the hydrophilicity of these thick films depends on the nature of the material. It is certain that thick organic films left in a dry state will revert to their native low energy state within a short time (days to weeks); see Kumar et al., 2008. However, samples which remain immersed in water after treatment remain water wet for many months, since the association of the surface hydroxyls with water prevents the surface relaxation seen in the dry state. To illustrate the reproducibility of the plasma and hydrophobing processes non-porous silica, calcite and mica flats were made hydrophobic, treated with crude oils, flushed with traditional solvents and then plasma cleaned again. Figure 1 shows the results for air-water contact angles on the range of substrates.

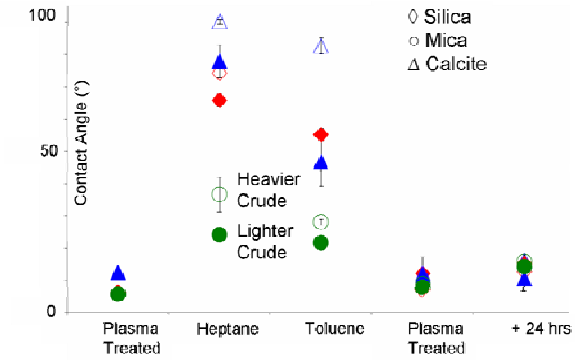

Figure 1: A sequence of contact angles with water in air on three substrates which were first plasma treated, then aged in crude oil, flushed with conventional solvents (heptane, toluene) and finally re-plasma treated. The contact angle after 24 hours in water is also reported. Open symbols denote results for heavier crude and filled symbols for lighter crude.

Strongly water-wet core is also used as a starting point for generating a mixed-wet core. The first step is to partially saturate the core with water. The water phase is allowed time to distribute in water films and depending on the water saturation, into smaller pores. The water is immobilized by rapidly freezing the core and the core is then immersed in a hydrophobing solution kept below 0°C. The water films remain immobile while the exposed surface becomes oil-wet. The mixed–wet core is then drained and flushed of residual hydrophobic agent while the water films remain frozen. The water is removed by oven drying the core at 110°C. Wettability indices for the mixed wet cores were measured using a modified Carter method (Okasha et al., 2007). This method normally uses 2 adjacent plugs saturated with water and oil and immersed in counterpart fluid baths. The pore volume of displaced fluid is measured - I_w and I_{nw} and WI = (I_w-I_{nw}). Here the volumes of fluid uptake by wetting and non-wetting fluids are measured on the same core. Samples of Fontainebleau sandstone and sucrosic dolomite were “designed” (based on the partial saturation of the core before freezing = water wet fraction) to have WI = -0.05 and 0.14. They were found to have WI = .08 and 0.16 respectively.

PORE SCALE DISTRIBUTION OF FLUIDS IN FLOODED CORES

This section describes the analysis of air-water drainage and imbibition displacement experiments on cores treated in the manner described in the previous section. This preliminary study was designed to validate the experimental and analysis procedures discussed above and to demonstrate the potential value of the fluid imaging data. A more comprehensive study of the effects of wettability on fluid displacements in reservoir cores using model and reservoir oil-brine systems is now underway.

Seven cores - three Fontainebleau sandstone, three sucrosic dolomite and one oomoldic grainstone – were used in the experiments. The cores were generally 5-6 mm in diameter and 15-20 mm in length. 3D images of the cores in dry and partially saturated states were obtained using the ANU micro-CT facility (Sakellariou et al., 2004) at voxel sizes down to ~3 microns. Images were taken from the central 6 mm region of the core (away from the ends). All images were composed of 2048^3 voxels. A new image registration technique (Latham et al, 2008) has made it possible to superpose, at voxel resolution, images of the same core images at different water saturations. This allows the pore scale distribution of the fluids in the core to be quantified. The water phase in all experiments was 0.1M CsI solution to enhance fluid contrast.

Samples	Diameter (mm)	ϕ_{exp}(%)	ϕ_{image}(%)	S_w^{exp}(%)	S_w^{image}(%)	k (mD)
Sucr. Dolo.	5.0	25.0	24.5	86/32	93/23	900
Oomoldic	5.0	18.1	19.1 (10.8)	49	53	80

Table 1. *Details of samples studied in drainage. Sample size is given in mm. The experimental porosity is based on MICP on the same subsample of core material imaged. Two drainage experiments on sucrosics dolomites are undertaken (two values reported). For oomoldic sample we report the total porosity after inclusion of the microporous fraction (see Knackstedt et al., 2007) and the resolved porosity (given in brackets). Experimental saturations(S_w^{exp}) and saturations measured from the image (S_w^{image}) are also given. Indicative permeabilities are also shown.*

Drainage Experiments

Details of the cores used for the drainage experiments are shown in Table 1. A strongly water-wet state was established for each core using the following procedure: 1) Plasma clean core as described above; 2) Heat shrink the core with a water wet porous frit (<1 micron pore size) at one end; 3) Overnight in vacuum oven at 85 degrees; 4) Plasma clean core for 15 minutes; 4) Saturate under vacuum with 0.1M CsI water; 5) Centrifuge in air to desired water saturation; 6) Seal off and allow core to equilibrate for 12-24 hrs; 7) Image on micro-CT facility. The different final water saturations for each of the drainage experiments shown in Table-1 were established in this manner.

Sucrosic Dolomite:

The imaged pore-scale air-water distributions for the sucrosic dolomite cores at high and low water saturations are shown in Fig.2. The core was first imaged dry and an equivalent pore network extracted from the image contained more than 50,000 pores and 120,000 throats. Information on the spatial distributions of pore/throat sizes, aspect ratios and coordination numbers were obtained from the networks. Images after drainage experiments were then obtained (Fig. 2(b,c)). Images are obtained away from the inlet/outlet of the samples and reasonably constant saturation observed in the field of view. Water saturations

in individual pores and throats are determined by overlaying dry and partially saturated 3D images with voxel registration. Fig 2(d) shows the distribution of the gas phase as a function of pore size on the image at low S_w. As expected the data shows a strong correlation between pore size and wetting phase saturation. The intermediate to large pores have low water saturations with the higher water saturations observed in the smallest pores.

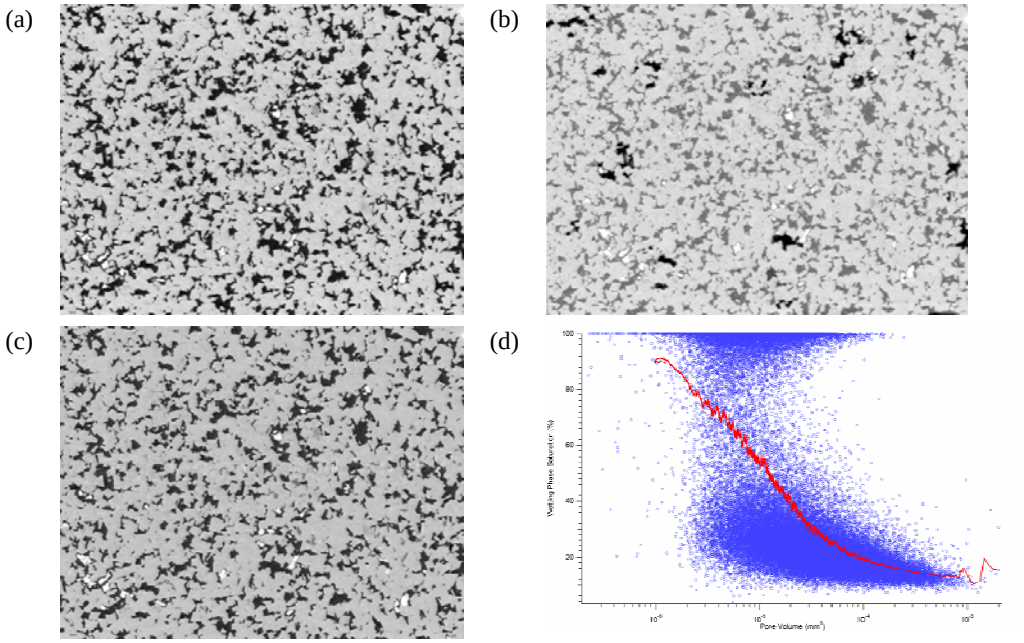

Figure 2: *Slices of 3D micro-CT images: (a) dry sample; (b) registered slice of flooded sample at S_w=93% (c) registered flooded sample at S_w=23%. (d) shows the distribution of the wetting phase saturation in individual pores for the S_w=23% sample. The blue points give a scatter plot of the local saturation within the pores and the red line gives a running average of the relationship between pore size and S_w.*

<u>Oomoldic grainstone:</u>

An image of the dry oomoldic grainstone core is shown in Fig. 3 (a). This core displays significant resolvable porosity in the form of molds. These pores are of size >100 microns. The *connectivity* of molds is often via a microporous matrix of cements between the molds. The microporous matrix has a strong influence on permeability and productivity of moldic grainstones. Fig. 3(c) shows MICP data for the sample. We note a bimodal throat size distribution with ~40% of the pore space accessible at throat sizes of >3 microns. The remainder of the pore space is only accessible through tighter throats. Fig. 3(b) shows the same slice in the rock after drainage to a saturation S_w =53%. A cluster of the larger moldic pores have been drained while others remain water filled. Fig. 3(d) shows the same experimental image with the wetting and non-wetting fluids highlighted.

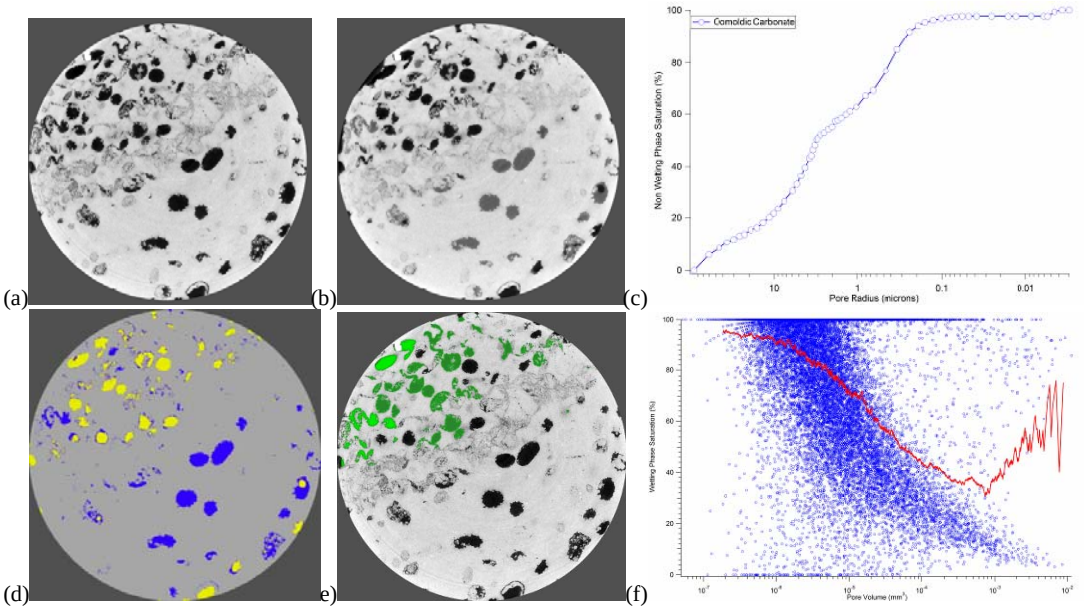

Figure 3: *Slices of 3D micro-CT image of the oomoldic grainstone; (a) dry sample; (b) registered slice of flooded sample at S_w~53%; (c) MICP data for sample; a bimodal throat size distribution is noted with ~40% of the porosity accessible at >3 microns and significant porosity accessible only via micropores. (d) highlights the regions experimentally drained (orange) at an effective throat radius of ~3 microns and (e) gives the image based distribution of connected pores at the image resolution. The distribution of the non-wetting phase is similar in the two images. (f) shows the distribution of the wetting phase saturation in individual pores. Unlike the well connected dolomite, some of the largest pores remain water saturated due to the lack of connectivity.*

The experimental drainage displacements are simulated by computations directly on the dry image or on the equivalent pore network to identify those pores which have been drained and those which remain undrained. The simulations are performed by defining locally for every point the diameter of the largest sphere which fully lies within the pore phase and covers that point (*covering radius*). Starting with the largest sphere and incrementing the sphere radius downwards (incrementing capillary pressure), the non-wetting phase saturation is measured as the subset of all spheres that have invaded the pore space. Fig. 3(e) compares the simulated fluid distributions at an effective pore entry radius of 3 microns with the imaged data. The correspondence between pores drained in the simulations (Fig. 3(e)) and those observed to be drained in the images (Fig. 3(d)) is encouraging.

Spontaneous Imbibition Experiments

The spontaneous imbibition measurements were carried out using three Fontainebleau sandstone (FB) and two sucrosic dolomite (SU) cores. The experiment was conducted by suspending the dry plug from a 0.1 mg accuracy balance and bringing the lower face of the plug in contact with a 0.1M CsI solution. The gas saturation is calculated from the measured water uptake. Since the cores are small (5-6 mm diameter) the uncertainties in the corrections for buoyancy and capillary entry effects are relatively large; we estimate that errors in the reported saturations are of the order of $\pm$10%. The two experiments for

the SU cores were carried out at water-wet and mixed wet (WI=0.16) conditions. Two of the FB cores were strongly water-wet and a third was at mixed-wet conditions (WI=0.08). In all cases images are in the center of the sample; away from the inlet/outlet of the samples. Reasonably constant saturation profiles are observed in the field of view.

Sucrosic Dolomite:

Sample 1; Mixed wet

We first discuss the SU core under mixed wet conditions (WI=0.16). In this experiment the initial uptake of water was rapid with the bulk of the water taken up within the first 3 minutes. The sample was left in contact with the water bath for an extended period (>24 hours) to ensure that the core equilibrated. The core was then imaged. The results of the experiments are shown in Fig. 4; a slice through the dry image is shown in (a) along with a registered slice after the spontaneous imbibition experiment (b). The residual gas phase is clearly evident from the image and highlighted in (c). The trapped gas phase saturation is 31%.

Imbibition is complex and imaging the resulting pore-scale distribution of fluids can assist in improving our understanding and modelling of the process. The imbibition of a wetting fluid into a porous media is influenced by rate, heterogeneity of the pore space and local pore geometry, which can lead to a wide variety of wetting patterns including site invasion percolation, cluster growth and flat frontal advance (Lenormand & Zarcone, 1984; Blunt & Scher, 1995). The complexity increases for spontaneous imbibition where the capillary number (*Ca*) is continually decreasing, and where the displacement front advances simultaneously at many locations - quasistatic rule based models do not apply. An added complication may be the mixed-wet nature of the core. Notwithstanding these complexities, the imaged saturation distributions shown in Fig. 4(c) show that the trapped gas phase is concentrated in the largest pores. This suggests that a simple percolation type mechanism may be relevant in describing the process (Wilkinson, 1984).

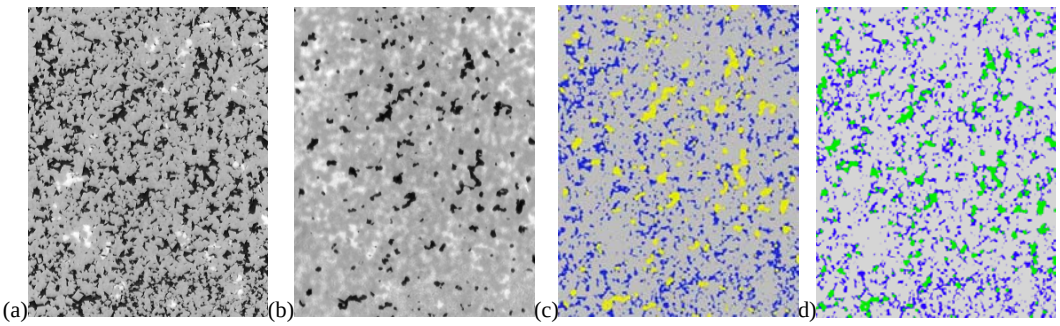

Figure 4: *(a) Slice of 3D micro-CT image of SU in dry state; (b) registered slice after spontaneous imbibition; (c) phase separation of pore space allows separation of water (blue) and residual gas (orange) on image in 3D. (d) shows an overlay of (c) with the distribution of the trapped phase (green) based on an ordinary percolation simulation on the 3D image having the same saturation as observed experimentally. The experimental distribution of the trapped gas phase correlates well to a model based on percolation.*

Samples	ϕ_{exp}(%)	S_{gr}^{EXP}(%)	S_{gr}^{Image}(%)	$S_{gr}^{Percolation}$(%)	Z
SU: MW	20.2	31	31	51	4.1
SU: WW	24.1	25	17	53	4.7
FB: MW	11.5	31	26	58	3.7
FB: WW, short	13.9	40	37	53	4.1
FB: WW, long	16.4	21	21	48	4.7

Table 2: Data for spontaneous imbibition runs. The porosity measured from image data are given in the second column. S_{gr}^{EXP} the experimentally measured (mass basis ±10%) for S_{gr}, S_{gr}^{Image} is the image based measurement of S_{gr} . $S_{gr}^{Percolation}$(%) definse the percolation threshold of the trapped gas phase based on the ordinary percolation model. Z gives the mean coordination of the resultant pore network model.

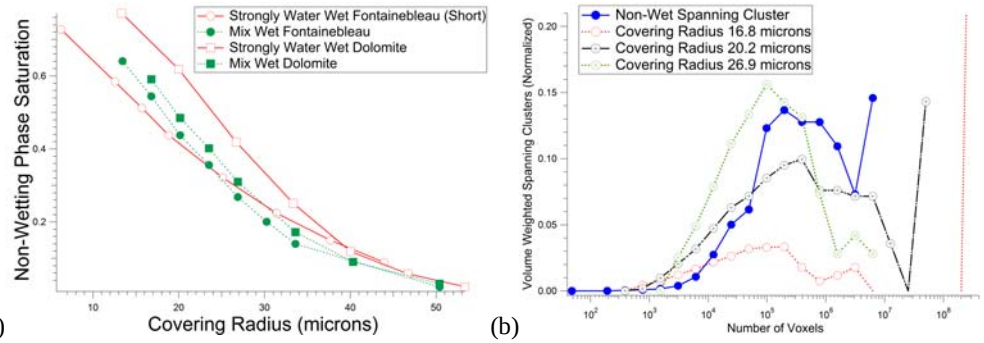

(a) (b)

Fig. 5:(a) Saturation of displaced fluid as a function of covering radius for SU and FB samples. (b) Distribution of trapped gas clusters from percolation theory and experiment for SU MW sample. The sample at a covering radius of 16.8 microns has a single cluster with >70% of the gas phase.

In a percolation-based model of an imbibition displacement the residual (trapped) gas saturation is formed when the displaced fluid (gas) stops percolating or becomes disconnected. This ordinary percolation threshold is easily determined on the 3D image data by incrementally removing spheres in the covering radius map from smallest to largest and tracking when the sphere map first disconnects. This is done on the original dry image and we find that the displaced fluid disconnects at an effective radius of ~16.8 microns. The saturation associated with this threshold is 51% which is considerably higher than the experimentally measured residual gas saturation of 31% (see Fig. 5(a)). It is interesting to note that when the percolation model saturation is reduced to match the measured residual gas saturation by further incrementing the covering radius map (see Fig. 5(a)) to an effective radius of 27 microns, the resulting distribution of gas is similar to that for the corresponding imaged experiment (compare Figs. 4(c) and (d)). Both samples exhibit broad residual gas cluster size distributions (see Fig. 5(b)).

Water wet: Sample 2

We now considered the SU sample under strongly water-wet conditions. In this experiment the initial uptake of water during the spontaneous imbibition experiment was extremely rapid (< 1 minute). The sample was again left in contact with the water bath for >24 hours to ensure equilibrium conditions. The results of the experiments are shown in Fig. 6. The imaged trapped gas phase saturation is now reduced, compared to the mixed wet samples, to S_{gr}=17%.

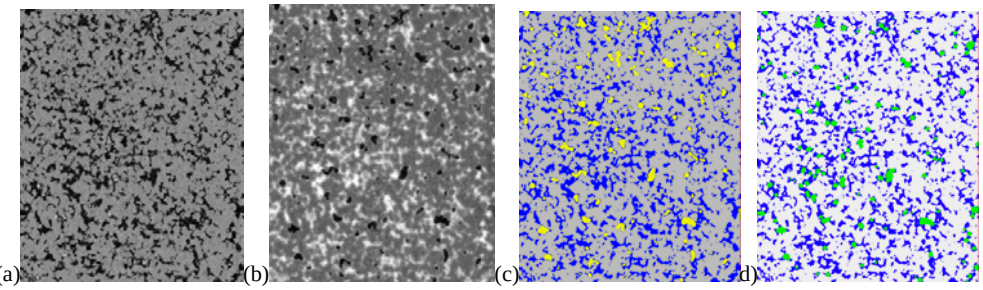

Figure 6: *(a)-(d) as in Fig. 4. On comparing (c) and (d) we again note that the experimental distribution of the trapped gas phase (orange in (c)) correlates well to a model based on simple percolation (yellow in (d)).*

For strongly water wet conditions with extremely rapid water takeup across a small sample, one might expect that the effective *Ca* is very large and the imbibition mechanism would approach a frontal drive with little trapping of the gas phase. We do note a significant reduction in the trapped gas phase saturation compared to the MW sample with the gas phase again concentrated in the largest pores. In a percolation based model, by choosing the covering radius map to have an effective radius of 33 microns the saturation of the percolation process agrees quite well with experimental observations (compare Fig. 6 (c) and (d)). In both sucrosic samples, no significant variation in saturation is observed with depth. Near the entry one might expect a more compact front; the ends of the cores seem to be sufficiently distant from the imaged regions.

<u>Fontainebleau Sandstone</u>

Mixed Wet: Sample 1

In this experiment the uptake of water during the spontaneous imbibition experiment was rapid (~2-3 minutes). The sample was left in contact with the water bath for 24 hours to ensure equilibrium conditions. The results of the experiments are shown in Fig. 7. The residual gas phase is clearly evident from the image. The trapped gas phase saturation is 26.1%. We again compare the fluid distribution to a percolation based model and again the saturation associated with the percolation threshold is significantly higher than that measured experimentally: ~58% vs 26% . However, by incrementing the covering radius map to an effective radius of 27 microns the saturation of the percolation process agrees quite well with experiment (compare Fig. 7(c) and 7(d)).

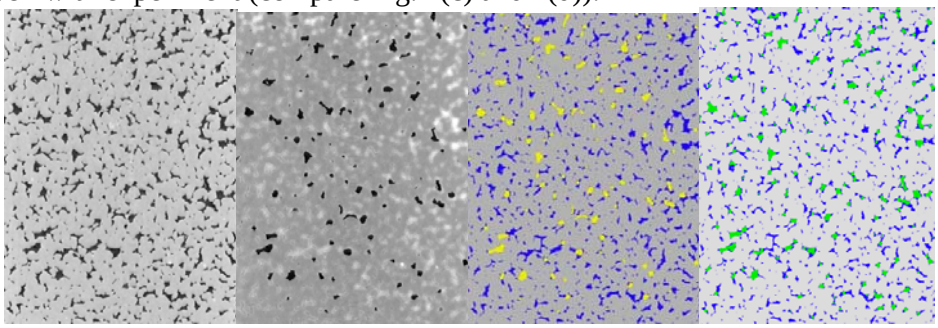

Figure 7: *As in Fig. 4 for WW Fontainebleau sandstone. From left to right, dry state; registered slice after spontaneous imbibition experiment; phase separation of pore space into water saturated (blue) and residual gas saturation (orange) and comparison to OP model (yellow) at equivalent saturation.*

Strongly water wet: Short vs. long equilibration times: Samples 2 & 3.
Two experiments on strongly water wet Fontainebleau sandstone were undertaken. Both samples were subsections from the same original core plug (ϕ=13.8%). In both cases the initial uptake of water during the spontaneous imbibition experiment was extremely rapid (< 1 minute). In the first experiment, the sample was removed from the water at the end of the fast imbibition process, all excess water removed, the sample sealed and immediately imaged. Images of the trapped gas saturation of the sample are shown in Fig. 8(a) and (b). The trapped gas saturation in this sample is measured as 36.9%. The residual (trapped) gas saturation estimation based on the ordinary percolation model; the point where the large pores stop percolating or become disconnected is 53% (Fig. 8(c)). In this case, the residual gas saturation more closely matches the percolation based model of an imbibition displacement. This result is slightly lower than the data presented by Hamon et al., 2001 who report extensive data for the porosity dependence of S_{gr} for water-wet Fontainebleau sandstone. Fig. 8 of their work shows that for ϕ~14%, S_{gr} ~40-50%.

The residual gas saturation data reported by Hamon et al., 2001 correspond to our *short contact time* data. They observed further reductions in gas saturation after this initial capillary dominated short period. For long equilibrium times the reduction in gas saturation was significant - e.g., S_{gr}; for ϕ~14% gave S_{gr} ~20-30% (Aissaoui, 1993).

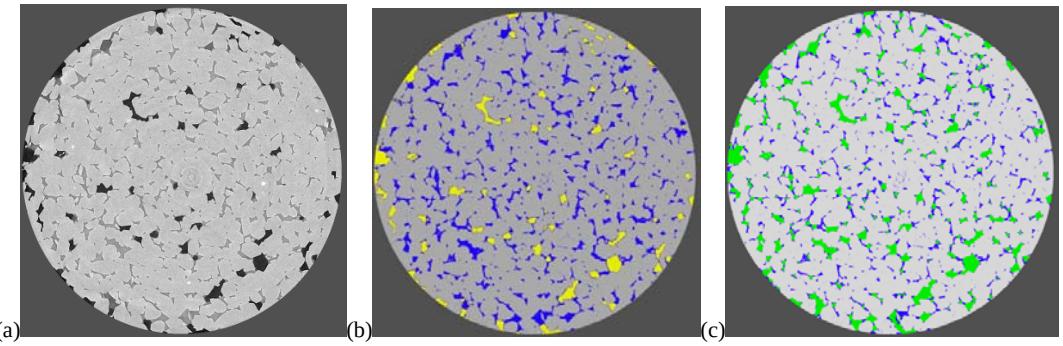

Figure 8: *(a) Fontainebleau sandstone sample after short contact time with water; (b) water saturated (blue) and residual gas saturation (orange) and (c) (yellow) comparison to OP model at equivalent saturation.*

In view of the above, a second spontaneous imbibition experiment was run on a different sub-sample (ϕ=16.4%). In this case the sample was left in contact with the water bath for 24 hours. The trapped gas saturation for this test was 24%. This is significantly lower than the corresponding saturation for the test where the sample was removed from the bath after the rapid initial imbibition. The result is consistent with previous experiments (see Fig. 8 of Hamon et al, 2001 and Aissaoui, 1993); ϕ~16%, S_{gr} ~25%.

Despite the differences in the value of S_{gr} after different equilibration times a percolation based model quite accurately describes the broad trapped cluster size distribution of the residual gas phase in both experiments.

CONCLUSION

- A cold water plasma core cleaning method is effective in cleaning reservoir cores to a strongly water-wet state. The method is highly reproducible and forms the basis of a technique to produce cores with well defined wettability states.
- Simple drainage and imbibition experiments on small cores coupled with high resolution CT-imaging of the same cores have clearly demonstrated that it is now possible to directly image fluid distribution in reservoir rocks at the pore-scale.
- Residual gas saturations and water saturations determined from imaged phase distributions at the pore-scale are in good quantitative agreement with laboratory measured residual gas saturations for spontaneous imbibition experiments and centrifuge drainage experiments for the same core plugs.
- Imaged fluid distribution data will be invaluable in testing the validity of network models used to predict multi-phase rock property data. Preliminary results suggest that percolation models for imbibition produce residual gas cluster size distributions which are similar to those imaged for the simple air-water system used in the present study.

ACKNOWLEDGEMENTS

The authors acknowledge the member companies of the Digital Core Consortium for providing funding support and the Australian Partnership for Advanced Computation for supplying computing resources.

REFERENCES

1. Aissoui, A. Etude theorique et experimentale de l'hysteresis des pressions capillaries et des permeabilites relatives en vue du stockage souterrain de gaz, Thesis Ecole des Mines de Paris (1983), 223 p.
2. Anderson, W.J., Wettability Literature Survey Part 2: Wettability Measurement, JPT, November 1996, pp. 1246-1262 (1986).
3. Blunt, M. J. and H. Scher. Pore level modeling of wetting, Phys. Rev. E, **52**, 6387-6403 (1995)
4. Hamon, G, K. Suzanne, J. Billiotte and V. Trocme, 2001. Field-wide variations of trapped gas saturation in heterogeneous sandstone reservoirs, **SPE 71524**, presented at 2001 SPE Annual Technical Conference, New Orleans.
5. Hirasaki, G, Rohan, J., Dubey, S and Niko, H, Wettability Evaluation during restored state core analysis, Society of Petroleum Engineers 20506, 1990.
6. Knackstedt, M, et al., Pore Scale analysis of electrical resistivity in complex core material, Proc. Of the Soc. Core Analysts, Calgary, Canada, September 2007, Paper
7. Kumar, M., T. J. Senden, S. J. Latham, et al. 2008. Designing for Mixed Wettability. In *2008 SPE Improved Oil Recovery Symposium*,Tulsa, Oklahoma: Soc. of Petroleum Engineers. SPE 113862
8. Latham, S, T. Varslot and A. P. Sheppard, Image Registration: Enhancing and Calibrating X-ray Micro-CT Imaging, Proc. of the Soc. Core Analysts, Abu Dhabi, UAE, October 2008, Paper A42.

9. Lenormand, R and C. Zarcone, 1984. Role of Roughness and edges during imbibition in square capillaries, **SPE 13264**. Presented at 59th Annual Technical Conference, Houston, 1984.
10. Morgan, W.B., Pirson, S.J., 1964. The effect of fractional wettability on the Archie saturation exponent. Presented at 5th SPWLA Annu. Logg. Symp., Midland, TX.
11. Morrow, N and Mason, G., 2001. Recovery of oil by spontaneous imbibition, Current Opin. In Coll. & Interf. Sci., **6**, 321-337.
12. Okasha, T, Funk, J and Al-Enezi, S., Fifty years of Wettability measurements in the Arab-D carbonates, in 2007 Middle East Oil and Gas Show, Bahrain, SPE105114.
13. Sakellariou, A., T.J. Senden, T.J. Sawkins, M.A. Knackstedt, A. Limaye, C.H. Arns, A.P. Sheppard, and R.M. Sok (2004): "An x-ray tomography facility for a wide range of mesoscale physics applications." U. Bonse (ed.): *Proceedings of SPIE* **5535**. Bellingham, WA, pp. 166-171.
14. Wilkinson, D (1984). Percolation in immiscible displacement, Phys. Rev. A, **34**, 1380-1391.
15. Zhang, D, Lui, S, Puerto, M, Miller, C.A. and Hirasaki, G, Wettability alteration and spontaneous imbibition into carbonate formations, J. Pet. Sci & Eng., **52**, 213-226 (2006).